

Nanoscale

Accepted Manuscript



This is an *Accepted Manuscript*, which has been through the Royal Society of Chemistry peer review process and has been accepted for publication.

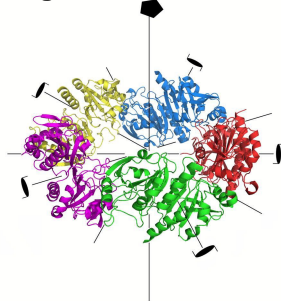
Accepted Manuscripts are published online shortly after acceptance, before technical editing, formatting and proof reading. Using this free service, authors can make their results available to the community, in citable form, before we publish the edited article. We will replace this *Accepted Manuscript* with the edited and formatted *Advance Article* as soon as it is available.

You can find more information about *Accepted Manuscripts* in the [Information for Authors](#).

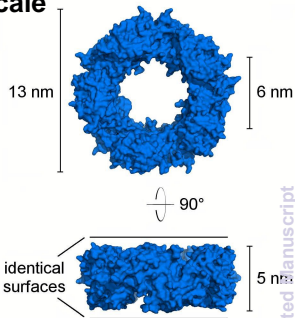
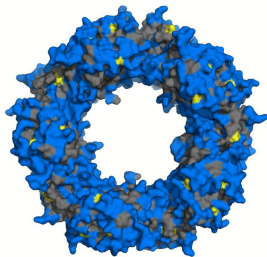
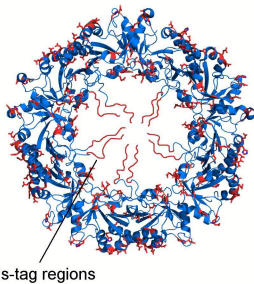
Please note that technical editing may introduce minor changes to the text and/or graphics, which may alter content. The journal's standard [Terms & Conditions](#) and the [Ethical guidelines](#) still apply. In no event shall the Royal Society of Chemistry be held responsible for any errors or omissions in this *Accepted Manuscript* or any consequences arising from the use of any information it contains.

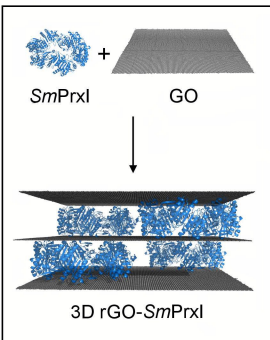
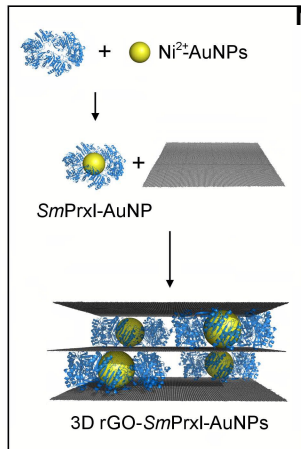
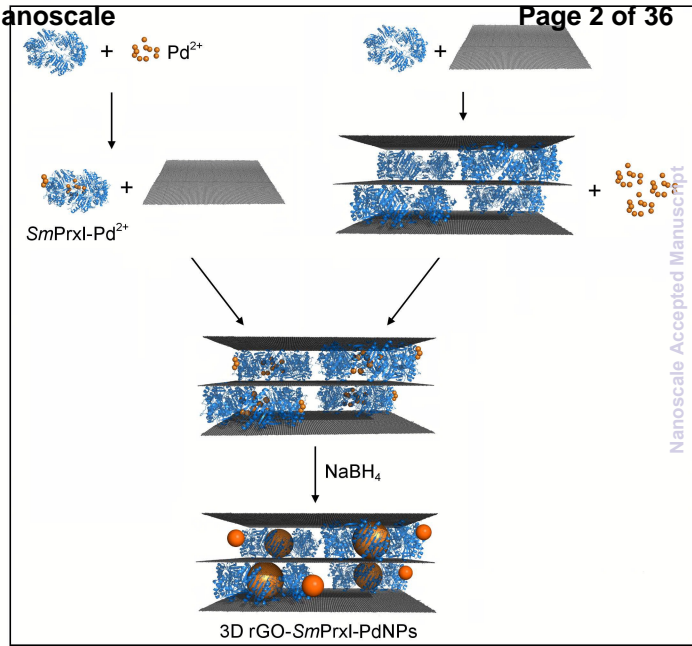
a

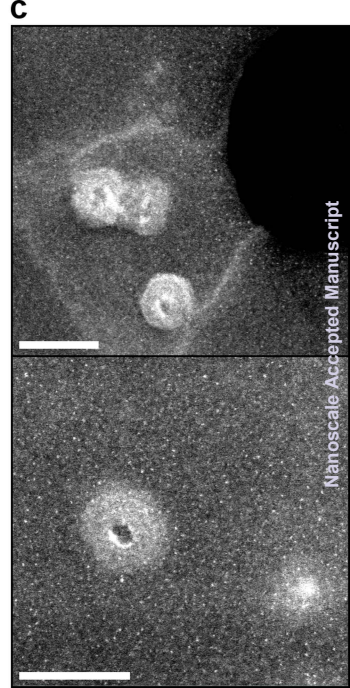
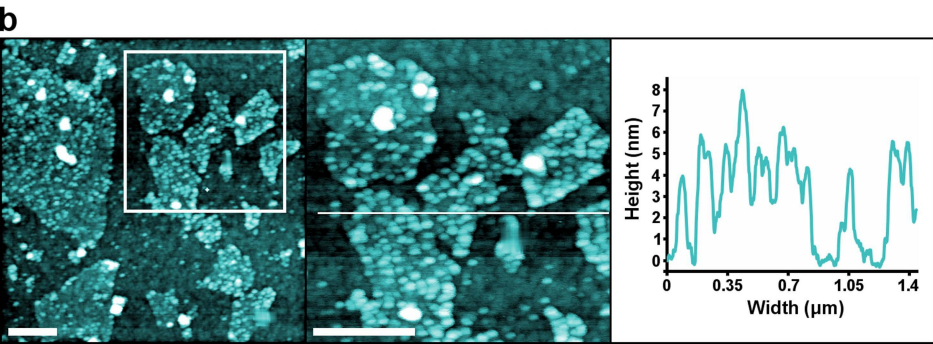
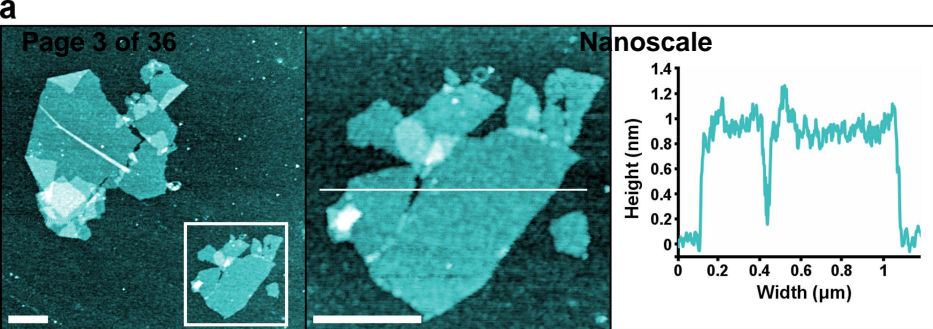
Page 1 of 36

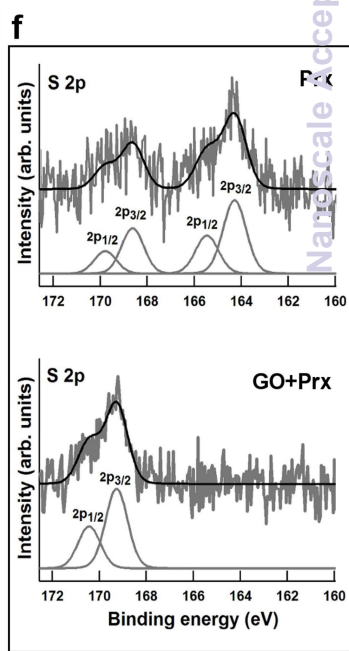
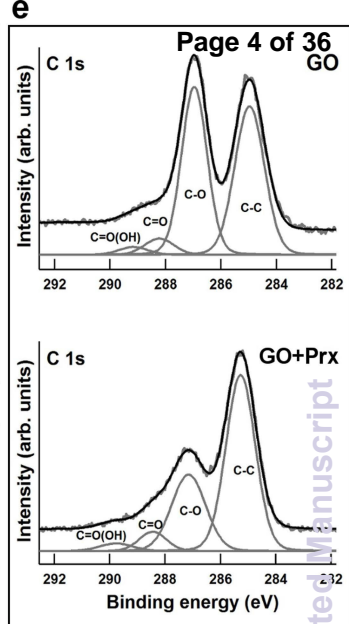
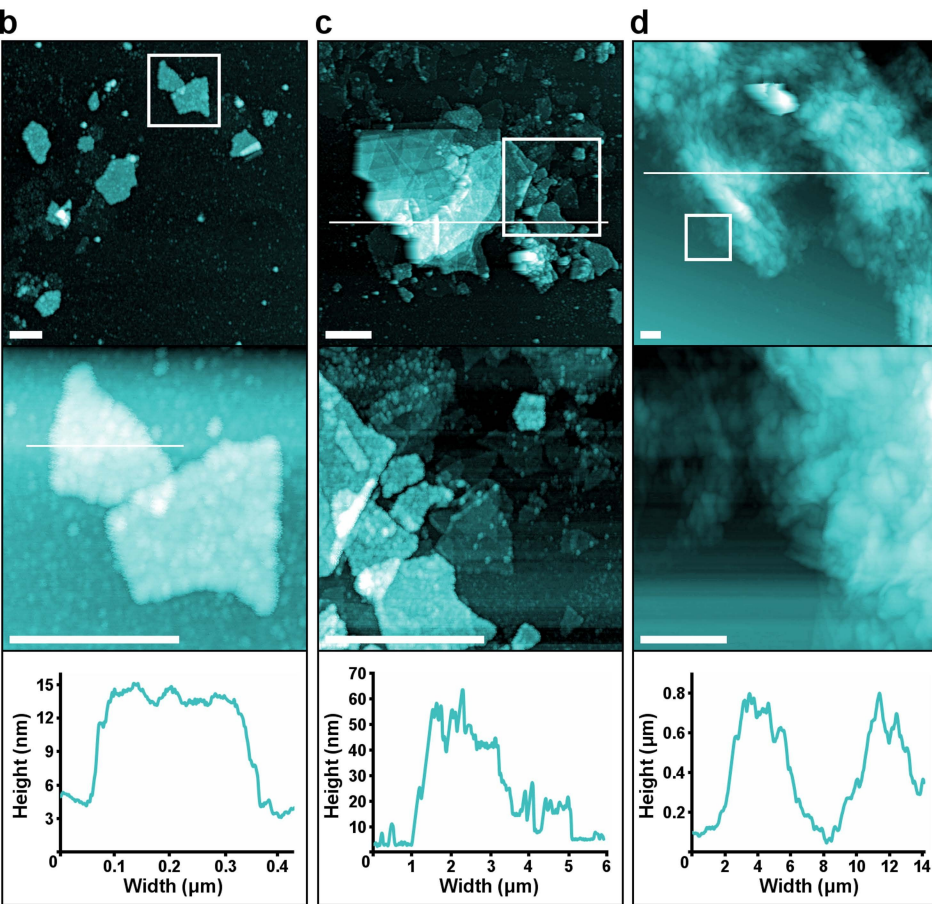
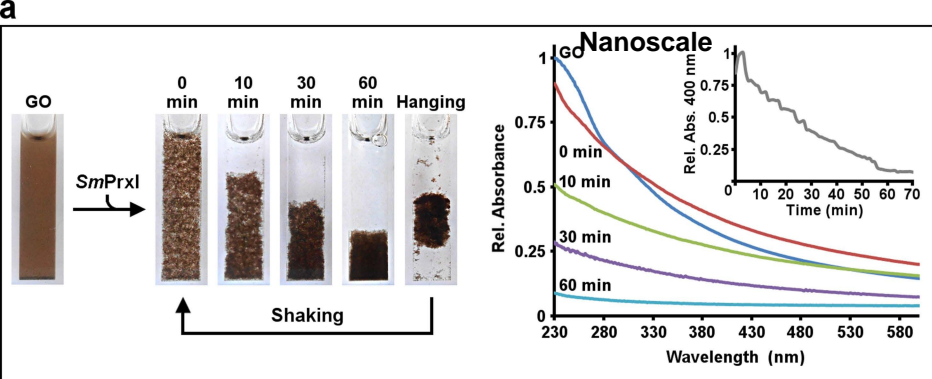


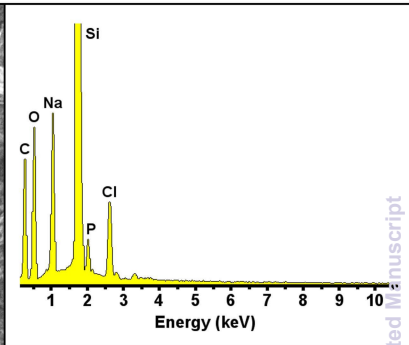
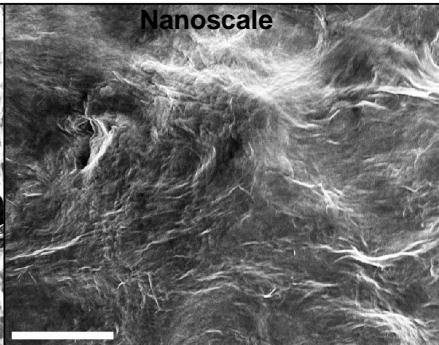
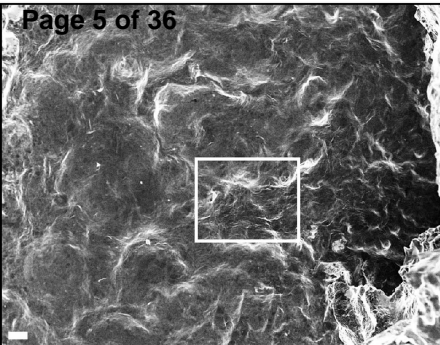
Nanoscale

b**c****d**

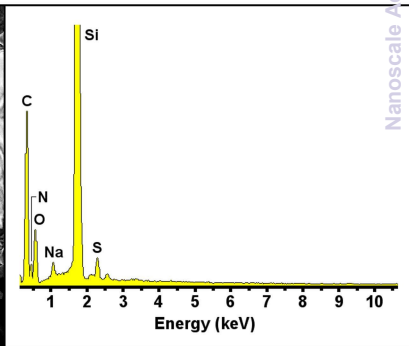
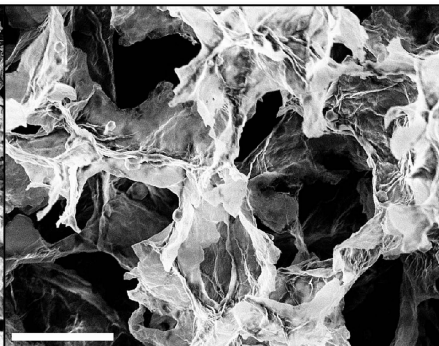
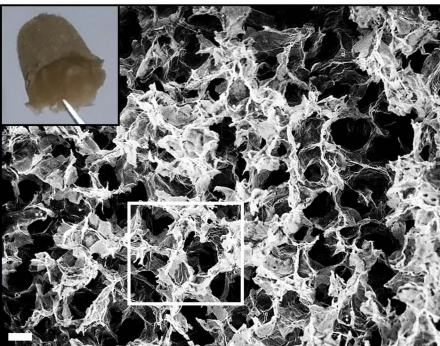
a**b****c****Nanoscale**

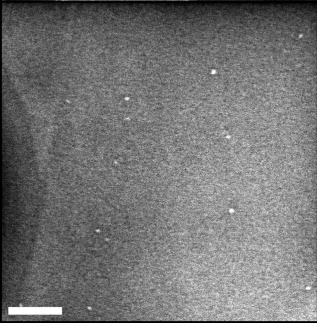
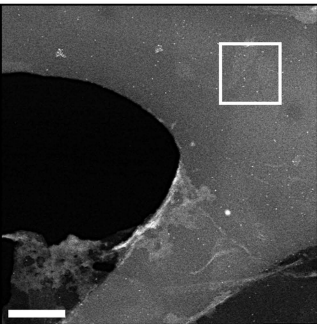
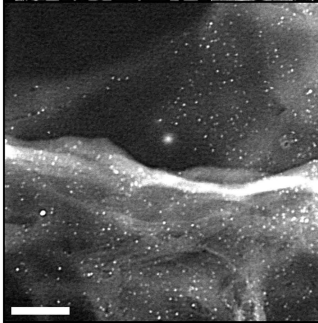
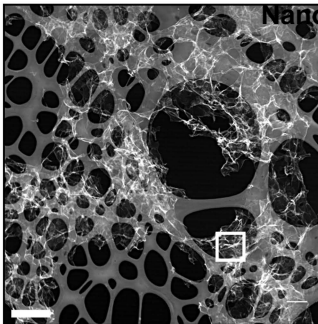
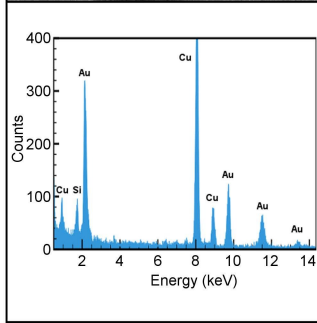
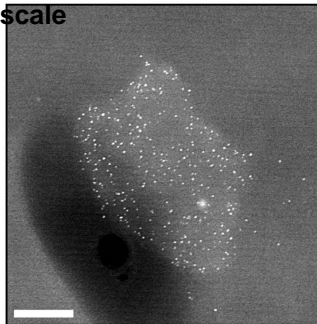
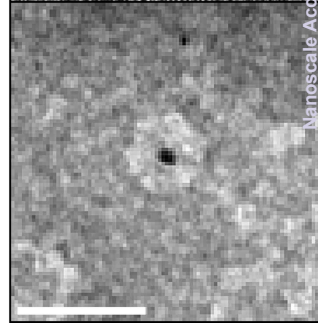
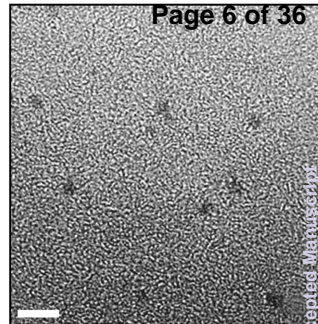


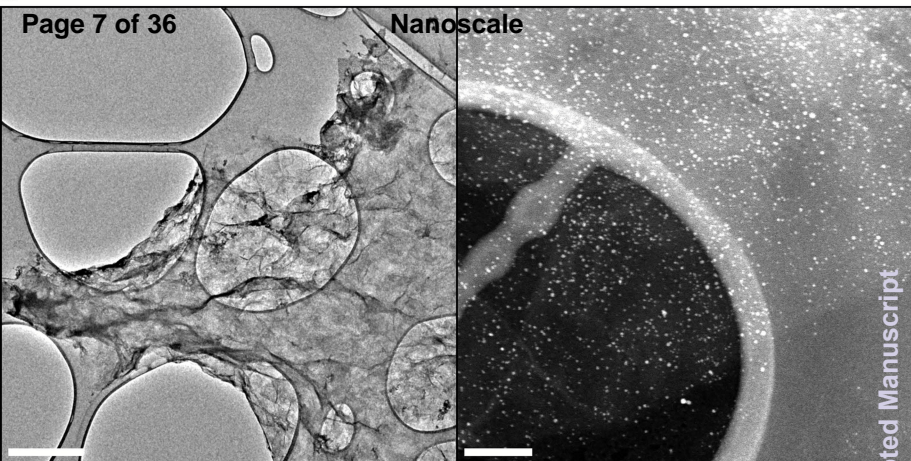




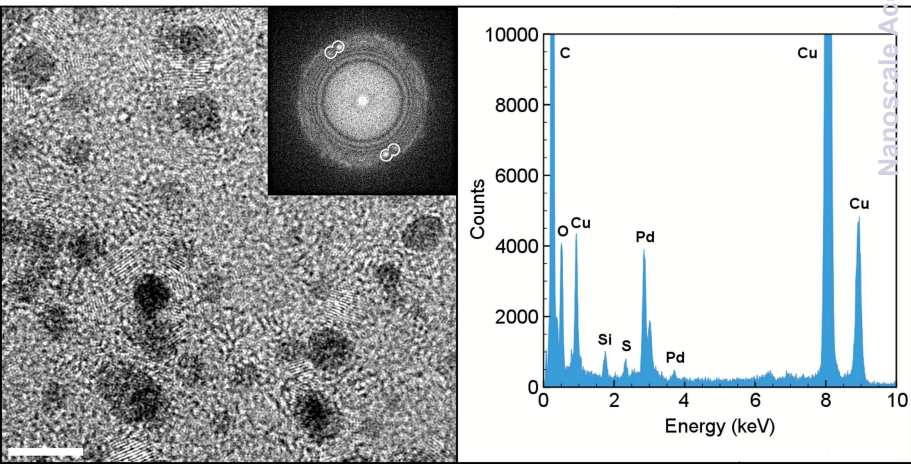
b

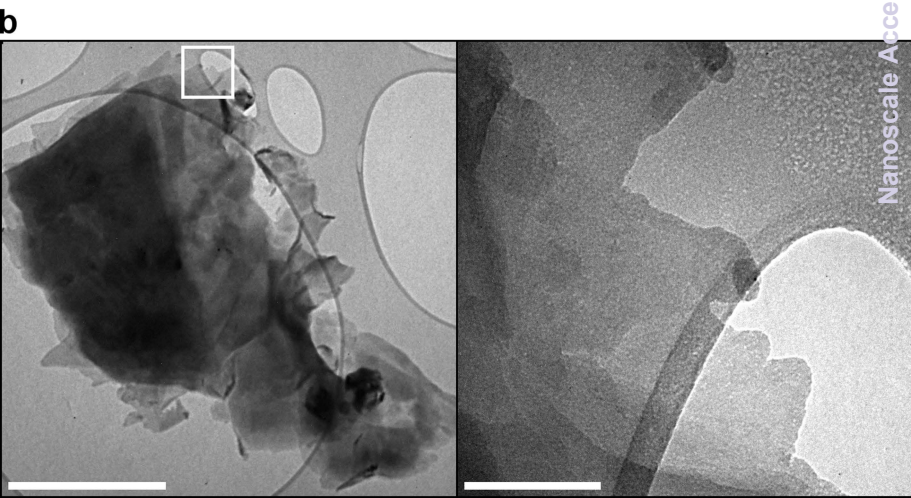
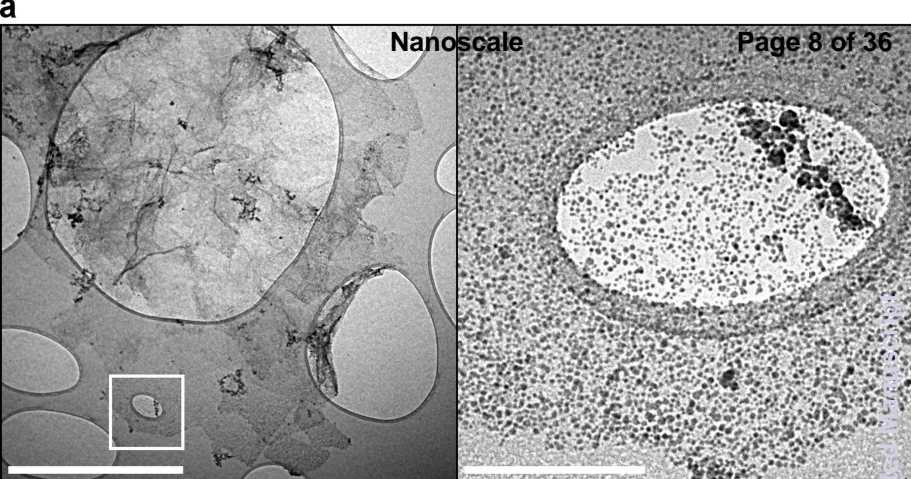


a**b****c****d**



b





Supramolecular self-assembly of graphene oxide and metal nanoparticles into stacked multilayers by means of a multitasking protein ring

Matteo Ardini¹, Giordana Golia¹, Paolo Passaretti¹, Annamaria Cimini¹, Giuseppina Pitari¹, Francesco Giansanti¹, Luana Di Leandro¹, Luca Ottaviano², Francesco Perrozzì², Sandro Santucci², Vittorio Morandi³, Luca Ortolani³, Meganne Christian^{3,4}, Emanuele Treossi⁴, Vincenzo Palermo⁴, Francesco Angelucci^{1*}, Rodolfo Ippoliti^{1*}

¹Dept. of Life, Health and Environmental Sciences, University of L'Aquila, Italy

²Dept. of Physics and Chemistry, University of L'Aquila, Italy

³National Research Council of Italy, Institute for Microelectronics and Microsystems, Bologna, Italy

⁴National Research Council of Italy, Institute for Organic Synthesis and Photoelectronics, Bologna, Italy

*To whom correspondence should be addressed:

Francesco Angelucci

Dept. of Life, Health & Environmental Sciences

University of L'Aquila

Via Vetoio, loc. Coppito, 67100 L'Aquila, Italy

Tel: +39 0862433787

Email: francesco.angelucci@univaq.it

Rodolfo Ippoliti

Dept. of Life, Health and Environmental Sciences

University of L'Aquila

Via Vetoio, loc. Coppito, 67100 L'Aquila, Italy

tel: +39 0862433286

Email: rodolfo.ippoliti@univaq.it

Abstract

Graphene oxide (GO) is rapidly emerging worldwide as a breakthrough precursor material for next-generation devices. However, this requires the transition of its two-dimensional layered structure into more accessible three-dimensional (3D) arrays. Peroxiredoxins (Prx) are a family of multitasking redox enzymes, self-assembling into ring-like architectures. Taking advantage of both their symmetric structure and function, 3D reduced GO-based composites are hereby built up. Results reveal that the “double-faced” Prx rings can adhere flat on single GO layers and partially reduce them by their sulfur-containing amino acids, driving their stacking into 3D multi-layer reduced GO-Prx composites. This process occurs in aqueous solution at very low GO concentration, *i.e.* 0.2 mg ml⁻¹. Further, protein engineering allows the Prx ring to be enriched with metal binding sites inside its lumen. This feature is exploited to both capture presynthesized gold nanoparticles and-grow *in situ* palladium nanoparticles paving the way to straightforward and “green” routes to 3D reduced GO-metal composite materials.

Keywords

Graphene oxide, ring-like protein, nanoparticles, three-dimensional material, self-assembly.

1 Introduction

Graphene, a carbon allotrope with a two-dimensional (2D) honeycomb-like structure, has been acclaimed as a cutting-edge material since its discovery.¹ Because of its noteworthy properties including electronic/thermal conductivity¹⁻⁵ and mechanical strength³, attracted and is still attracting major interest. Moreover, graphene's benefits have further expanded after obtaining related materials such as graphene oxide (GO)⁶ that, differently from graphene, features tunable electro-optical and chemical properties, high hydrophilicity and ease of production and functionalization.⁷ For instance, the benefits of using GO have already been demonstrated for gas sensing⁸, large-scale and cost-effective manufacture of composite materials^{6,9} and the production of nano-bio materials¹⁰. Yet the possibility of obtaining reduced GO (rGO) by processing contributed greatly to its outstanding potential, as rGO can partially restore the properties of graphene while enabling its dispersion in surfactant-free solution^{11,12}.

However, using graphene for practical applications remains to be fully realized. One main issue is the integration of its 2D structure into accessible and scalable three-dimensional (3D) materials, a need that has inspired a growing field of research.¹³ For instance, hydro- and aerogels¹⁴ represent low-weight, soft, porous materials comprising a 3D network of carbon layers with interstitial spaces filled by solvent or air, and they have been proposed for applications in optoelectronics¹⁵, regenerative medicine¹⁶ and energy storage¹⁷. Molecular self-assembly represents an incisive strategy for building 3D graphene with defined architecture.¹⁸ Another recent research area aims at obtaining graphene-based composites enriched with metal nanoparticles (NPs) which display synergistic relationships between their components, yielding new "nanoreactors" with enhanced chemical-physical properties.^{12,19} However, some problems arise when graphene is functionalized with metal NPs due to both the difficult process of adsorption of preformed NPs onto the carbon surface²⁰ and the uncontrolled size and morphology upon *in situ* synthesis leading to highly heterogeneous products not suitable for applications requiring mono-dispersed material, such as catalytic reactions²¹.

Proteins are biopolymers with different shapes and properties that are able to interact with both GO and rGO through weak interactions due to their exposed hydrophobic and/or hydrophilic surfaces.²² Typical 2-Cys Peroxiredoxins (Prx) are enzymes with redox and molecular chaperone activity, that is the ability to keep non-native proteins in solution by means of the exposure of sticky

hydrophobic surfaces. Under physiological conditions, ten Prx subunits self-assemble into ring-like complexes with thickness, internal and external diameters of 5, 6 and 13 nm, respectively (Figure 1, PDB code: 3ZTL).^{23,24} This architecture arises from 5 homodimers assembled such that their 180° symmetry axes are perpendicular to the 5-fold rotational symmetry axis of the ring (Figure 1a). Thus, the exposed surfaces at the top and bottom of the ring plane, where the amino acids responsible for the redox and chaperone activity lie, are structurally and chemically identical (Figure 1b-c).²⁵ This peculiar assembly gives the Prx ring a “double-faced” appearance. Proteins, in general, are endowed on their surfaces with several amino acids, such as glutamic/aspartic acids and histidines, capable to bind metal ions;²⁰ moreover, here the N-terminal of each Prx subunit is engineered by adding extra amino acidic residues (Supporting Figure 1), which lie inside the ring lumen providing additional metal binding sites within the same protein scaffold (Figure 1d).²⁶

We demonstrate how the typical 2-Cys Prx I from *Schistosoma mansoni* (*SmPrxI*) is able to (i) adhere flat on GO, (ii) partially reduce its surface inducing GO aggregation, and (iii) facilitate doping of the resulting microporous 3D composite with presynthesized gold NPs (AuNPs) or *in-situ* generated palladium NPs (PdNPs), acting as a support for metal deposition (Figure 2). This synthetic route to 3D rGO-NPs composites is unique and feasible yet “green” and exploits the structural and functional properties of *SmPrxI*, *i.e.* (i) the sticky and redox-active surfaces, (ii) the “double-faced” structure and (iii) the surfaces available for metal binding.

2 Experimental

2.1 Bacterial culture, protein expression and purification. *SmPrxI* was produced as N-terminal histidine-fused protein as previously published.²⁶ Briefly, recombinant BL21(DE3)pLysS bacteria (Novagen) were grown in selective LB medium (Sigma-Aldrich) and the protein expression induced with IPTG (Sigma-Aldrich). A clarified cell extract was harvested after sonication followed by ultracentrifugation and loaded onto a Ni²⁺-equilibrated column on-line with an ÄKTAprime plus system (GE Healthcare). *SmPrxI* was stripped from the column with a gradient of imidazole (Sigma-Aldrich) and its purity assessed through non-native electrophoresis in polyacrylamide (Sigma-Aldrich). The protein concentration was estimated by spectrophotometer based on a 280 nm extinction coefficient of 25000 M⁻¹ cm⁻¹ and a decamer ring molecular weight of 250 kDa²³. Finally,

the preparation was sterile filtered using a 0.45 μm filter membrane (MDI Membrane Technologies, LLC) and stored up to 4 months at 4 $^{\circ}\text{C}$ until use. Before using for experiments, *SmPrxI* was dia-filtered against the experimental buffer through 3500 rpm centrifugation at 10 $^{\circ}\text{C}$ using 30 kDa cut-off filter devices (Millipore). All reported *SmPrxI* concentrations throughout the text refer to the ring complex.

2.2 UV-VIS spectrophotometry. Spectrophotometric measurements were carried out by means of a Cary-60 UV-VIS spectrophotometer (Agilent Technologies) using a quartz cuvette with 0.5 cm light path (Hellma). Optical spectra were acquired at room temperature (23 $^{\circ}\text{C}$) in the 230-600 nm wavelength range with a fast scan rate. For kinetics measurements samples were analyzed with 1 min cycle time without stirring. All absorbance readings were taken at least three times.

2.3 Assembly of the GO-based 3D composite. The colloidal composites were obtained by a mixing technique as described here. GO was obtained as described²⁷ and/or purchased from Graphene Supermarket. To produce the GO-*SmPrxI* composite 0.3 mg ml^{-1} GO was dissolved in 20 mM sodium phosphate buffer (PanReac AppliChem) pH 7.5 within a quartz cuvette with 0.5 cm light path. The solution was vigorously shaken using a vortex apparatus (Velp Scientifica) to evenly dissolve GO prior to add 0.6 μM *SmPrxI*. Upon protein addition, the resulting mixture was shaken again before incubating at room temperature (23 $^{\circ}\text{C}$) using an orbital shaker (Ika) rotating at 320 rpm. In parallel, a control sample of protein-free GO was prepared and treated. A similar procedure was performed to produce the AuNPs-doped GO-*SmPrxI* material. In this case, 0.6 μM of 1.8 nm AuNPs with Ni^{2+} -NTA functionalities (Nanoprobes) were pre-mixed for 10 min with the addition of 0.6 μM *SmPrxI* (1AuNP per protein ring) in buffer containing 20 mM imidazole (Sigma). This strategy has been successfully used to produce *SmPrxI*-AuNP adducts taking advantage of the strong interaction between the histidine residues located at the ring cavity and the Ni^{2+} ions tethered on the nanoparticle's surface. Imidazole was proven to modulate such an interaction, thus avoiding the formation of amorphous insoluble aggregates.²⁶ The *SmPrxI*-AuNP mixture was shaken by vortex and centrifuged for 5 min at 12000 rpm prior to mixing the resulting supernatant with 0.3 mg ml^{-1} GO and shaking again before incubation. As a control sample, a protein-free solution of GO-AuNPs was made. After 0, 10, 30 and 60 min incubation the absorbance spectra of all samples were collected in a range of 230-600 nm.

2.4 Chemical reduction of the GO-based composites. Chemical processing of GO into rGO was achieved through reduction with NaBH_4 as follows. The composites were first washed by 5 min centrifugation at 12000 rpm and the resulting pellets were suspended in the respective fresh buffer and shaken by vortex. Then, the mixtures were left incubating until reconstitution of the original material prior to adding 15 mM NaBH_4 (Sigma-Aldrich) and incubating again for 16 h under orbital shaking at 320 rpm. Due to the effect of NaBH_4 increasing the rigidity of the GO material after reduction to rGO¹¹, no vigorous shaking or pipetting was applied to the samples to avoid excessive breakage of the final material. The excess of reducing agent was removed by several washing steps through centrifugation followed by suspension of the pellets in fresh buffer.

2.5 Atomic Force Microscopy (AFM). The surface properties of the GO-based composites were explored by AFM imaging. Depending on the features to be analyzed, specimens were prepared differently as follows. For a first analysis, very thin specimens were made by dropping 30 μl of 0.2 mg ml^{-1} GO in 20 mM sodium phosphate buffer pH 7.5 onto a 1 cm^2 hydrophilic SiO_2 substrate pre-treated with piranha solution, followed by 1 min spin-coating at 2200 rpm. Then, 3 μl of a 0.08 μM *SmPrxI* in buffer were deposited by drop-casting, quickly dried with a mild nitrogen stream, and exhaustively rinsed with ultra-pure water before drying again. For a second analysis, thicker specimens were made to distinguish other morphological features. In this case, 0.02 mg ml^{-1} GO and 0.04 μM *SmPrxI* were mixed, shaken by vortex and 3 μl of the mixture was immediately dropped onto the substrate followed by rinsing and drying. Images were captured using a Digital D5000 scanning probe microscope (Veeco) placed in a dry room and provided with an antimony-doped silicon NCHV tip with approximately 9 nm curvature radius, resonance frequency between 344 and 371 kHz, and spring constant between 20 and 80 N m^{-1} (Bruker). The scanning tip was moved in air in tapping mode on a 5 μm^2 sample area at a 1 Hz scan rate according to a set point amplitude of 1.1-1.3 (proportional and integral gains were properly tuned for each sample). All captured images were finally visualized and processed using the modular software Gwyddion v2.37.

2.6 Scanning Electron Microscopy (SEM) and Energy Dispersive X-Ray Spectrometry (EDS). The overall 3D morphological features of the GO-based composites were studied through SEM analysis by means of a LEO 1530 scanning electron microscope (Zeiss-Gemini). Before

observations, all samples were subjected to a 3 h lyophilization treatment by freeze-drying using a VirTis Bench Top 2k apparatus (SP Industries, Inc). This procedure was carried out to guarantee complete removal of water in the samples without significantly altering their architecture. The obtained lyophilized materials were cut then fixed with glue on a 1 cm² SiO₂ substrate before performing the analysis. All images were acquired under 10⁻⁶ Torr vacuum using an accelerating voltage of 5-10 kV. Due to the absence of any stain on the protein and its extremely small dimensions (13 nm diameter), a SEM XL-30-CP microscope provided by a thin-window EDAX DX4 system for EDS X-ray microanalysis was used to reveal the presence of the protein components. With this aim, the most representative elements such as carbon, nitrogen, oxygen, sodium, phosphorus, chloride, silicon and sulfur were sought.

2.7 X-ray Photoelectron Spectroscopy (XPS). 6 µl of GO (0.3 mg ml⁻¹), *SmPrxI* and GO+*SmPrxI* solutions were respectively drop-cast on Au (100) substrates. The Au (100) substrates were previously cleaned with a 3:1 mixture of NH₄OH and H₂O₂ at 60 °C. XPS spectra were acquired with a PHI 1257 spectrometer equipped with a mono-chromatic Al K α source (h ν = 1486.6 eV) with a pass energy of 11.75 eV, corresponding to an overall experimental resolution of 0.25 eV. The acquired XPS spectra were fitted with Voigt line shapes and Shirley backgrounds and aligned to the 4f_{7/2} core level peak of the Au substrate at 84 eV. The C 1s core level spectrum of the GO after interaction with *SmPrxI* was calculated by subtracting the Prx C 1s spectrum after normalization from the GO+*SmPrxI* C1s spectrum. The Prx S 2p core level spectra were fitted with doublets related to the 2p_{3/2} and 2p_{1/2} spin-orbit splitting.

2.8 Batch Pd²⁺ adsorption experiments using thioglycolic acid (TGA). Considering its polyHis-fused inner surface, the *SmPrxI* ring was assessed for its adsorption of Pd²⁺ ions. This was accomplished using the organic acid TGA, which is able to bind Pd²⁺ forming a colored TGA-Pd²⁺ complex (2:1 molar ratio) whose amount can be estimated by spectroscopy.²⁸ A buffered solution of 1 mM (NH₄)₂PdCl₄ (Sigma-Aldrich) was mixed with 0.6 µM *SmPrxI* (>1600Pd²⁺ per protein ring) and left to react for 5 min under magnetic stirring at room temperature prior to ultra-centrifugation for 10 min at 10000 rpm. Then the sample supernatant was diluted 4-fold in borate buffer pH 9.5 (Fluka) before mixing with an excess of 3 mM TGA (Sigma-Aldrich). The solution was immediately analyzed by recording the optical absorbance in the 230-600 nm range within a quartz cuvette with

1 cm path length to reveal the presence of unbound Pd²⁺. The concentration of unbound palladium was estimated by a calibration line as described.²⁹ The ion retention ability of the Pd²⁺-loaded *SmPrxI* was also investigated. For this purpose, the *SmPrxI*-Pd²⁺ pellet obtained from the ultra-centrifugation step (see above) was extensively washed by evenly suspending it in fresh buffer followed by ultra-centrifugation and its supernatant assessed through the TGA-based assay. At the same time, a control protein-free sample made by 1 mM (NH₄)₂PdCl₄ and 0.3 mg ml⁻¹ GO (~1:1 weight ratio) was similarly treated to be assessed with TGA.

2.9 *SmPrxI*-supported growth of PdNPs on GO. Based on the *SmPrxI* ring's ability to firmly interact with divalent metals, *in situ* growth of PdNPs was accomplished on GO layers through chemical reduction of Pd²⁺ onto the protein support. In this case, 1 mM (NH₄)₂PdCl₄ in buffer containing 40 mM imidazole was mixed with 0.6 μM *SmPrxI* (>1600Pd²⁺ per protein ring) under magnetic stirring for 5 min at room temperature before adding 0.3 mg ml⁻¹ GO. The thus-obtained GO-*SmPrxI*-Pd²⁺ mixture was quickly stirred by vortex and ultra-centrifuged for 10 min at 10000 rpm. The resulting pellet was uniformly suspended in fresh imidazole-free buffer and its supernatant assessed through the TGA-based spectroscopic method for the Pd²⁺ content (see above). The pellet was extensively washed with imidazole-containing buffer to rinse away any Pd²⁺ ions and/or GO molecules not bound to the proteins and the supernatant was analyzed through the TGA-based assay. The suspended pellet was left incubating for 1 h at room temperature under orbital stirring until the formation of the aggregate was achieved prior to inducing chemical reduction through the addition of 50 mM NaBH₄ (Sigma-Aldrich) and 1 h incubation.

2.10 Scanning Transmission Electron Microscopy (STEM), Transmission Electron Microscopy (TEM) and Energy Dispersive X-ray Spectrometry (EDS). The 3D GO functionalized with both AuNPs and PdNPs was analyzed by means of STEM, TEM and EDS. Samples were observed by a FEI Tecnai F20 ST microscope, operating at 120 keV and the images were captured with a Gatan MSC794 camera. In the STEM modality, the images were acquired with a High Angle Annular Dark Field FISCHIONE detector, and the microanalysis was performed with an INCA EDS detector. In the case of the 3D GO functionalized with PdNPs, the samples were also observed with a CM-100 electron microscope (Philips) equipped with a tungsten filament operating at 80 kV. The 3D GO+*SmPrxI*+AuNPs was prepared as follows: 400 μl 0.3 mg ml⁻¹ GO washed with

isopropanol and water was mixed with 0.6 μM AuNPs and 0.15 mg ml^{-1} *SmPrxI* in phosphate buffer at pH 7.4. The resulting material was washed 3 times with bi-distilled water and deposited on a holey grid (Agar Scientific). A similar sample was prepared without the protein. The grids were dried for 1 h under ultra-high vacuum before STEM or TEM analysis. After NaBH_4 reduction the 3D GO+PdNPs, prepared as above, was washed twice with phosphate buffer at pH 7.4 to rinse the excess NaBH_4 and an aliquot of 20 μl was dropped onto a holey carbon grid (Agar Scientific). After washing with bi-distilled water the grid was dried for 1 h under ultra-high vacuum. Specimens were observed by TEM and STEM. Likewise, a protein-free control sample made by 0.3 mg ml^{-1} GO and 1 mM $(\text{NH}_4)_2\text{PdCl}_4$ was similarly treated and analyzed. Estimations of the size distribution and number of metal NPs have been obtained through the image software ImageJ v1.47a as previously reported²⁶, according to the following parameters: particle circularity= 0.9-1, area bin range= 0.4-30, area bin width= 1.

3 Results and Discussion

3.1 GO-*SmPrxI* interaction. The binding between GO and *SmPrxI* was investigated by atomic force microscopy (AFM) and transmission electron microscopy (TEM). A thin specimen suitable for AFM surface analysis was prepared by spin-coating GO on a SiO_2 substrate followed by dropping *SmPrxI* on top. Figure 3 reports the results of this morphological and structural characterization. Before the protein deposition, the GO molecules were imaged with AFM as single mono-atomic layers diffused all over the substrate. Among them, rare double- and triple-layer stacks, likely formed through spontaneous layer-by-layer deposition, were also found. All layers displayed a smooth planar surface with height values of $\sim 0.9\text{-}1$ nm (Figure 3a) in agreement with the typical known dimensions of GO³⁰, even though large variability in lateral size was noticed (0.3-1 μm , data not shown). After dropping *SmPrxI*, the planar surface of GO was no longer fully accessible for imaging as it was quite evenly coated by roundish protein particles with only a small amount attached to the underlying SiO_2 substrate. Confirming previous data²⁶, all the particles were ~ 20 nm wide, fitting with the known external diameter dimension of the decamer ring-like *SmPrxI* structure (see Fig 1b; PDB code: 3ZTL)²³. The higher diameter measured by AFM with respect to the one determined by X-ray crystallography (Figure 1b) was due to tip convolution effects, due to the large

tip curvature radius (~ 9 nm)³¹. Most of the protein rings had a mean height of 5.1 nm (sd= 0,78 nm) corresponding to the ring thickness value, thus suggesting a flat arrangement on the carbon plane. By contrast, only a few taller structures with ~ 12 -20 nm heights, probably vertically aligned or aggregate rings, were observed. Because of the presence of such a protein coating, the surface of GO became highly pitted, reaching ~ 6 nm height values, fitting with the dimension of a GO-*SmPrxI* architecture (Figure 3b). TEM investigation (Figure 3c) revealed the morphology of the GO-*SmPrxI* composites. TEM samples were prepared by drop-casting a water solution of GO over standard holey carbon film grids, then adding the *SmPrxI* solution and drying under vacuum. Samples were imaged at 120 kV in scanning transmission mode (STEM). Figure 3c shows individual ring proteins, confirming the flat morphology over the GO flake. However, the number of *SmPrxI* rings onto GO observed by STEM analysis was considerably smaller than that found by the AFM measurements most likely because of their electron-beam sensitivity that could quickly cause serious structural damage to the protein³².

3.2 *SmPrxI*-induced self-assembly and reduction of GO. The interaction of *SmPrxI* with GO was investigated by mixing experiments in aqueous buffer at pH 7.5 (Figure 4). Given its hydrophilic behavior, GO was easily dissolved to become a light brown solution that remained soluble for several hours before undergoing very slow precipitation. Upon addition of *SmPrxI* followed by vigorous shaking, the mixture quickly became highly coagulated as GO clumped into visible particles. Following incubation, the mixture underwent further aggregation to form a larger dark brown colloid, and slowly sank to the bottom of the cuvette in about 60 min (Figure 4a). Shaking caused disassembly of the so-formed colloid into separate particles, but these readily clumped again to form the original soft matter, suggesting a reversible self-assembly process. Despite its softness, the colloid could be entirely suspended in solution as a globular mass, indicating structural compactness. As a consequence, the process led to almost full phase separation between the buffer solvent and the colloidal matter. The gelation process was followed on the fly by measuring the UV-Vis light scattering caused by the GO clumping. The initial protein-free GO solution showed an intense broad optical density, but following mixing with *SmPrxI* remarkable scattering of light was recorded due to the formation of the clumped GO particles. Then, the absorbance of the mixture progressively decreased indicating the loss of soluble GO during precipitation. Notably, the final absorbance spectrum recorded after 60 min incubation was almost

zeroed indicating that neither GO nor *SmPrxI* were present in solution due to co-precipitation at least in the concentration range explored (Figure 4a). The so-obtained GO clumps were analyzed by AFM to gain insights into their structure. To this end, the analysis was performed on the GO clumps formed at the early stages of mixing with *SmPrxI*, dropped on a SiO₂ substrate. As expected, images showed a very heterogeneous population of GO-*SmPrxI* hybrid composites. Among the smallest ones, complexes made by single or partially overlapped GO layers with several protein rings all over their surfaces were found. Accordingly, these complexes showed a highly rough surface due to the presence of the protein coating and a height value of ~ 10 nm, suggesting a *SmPrxI*-GO-*SmPrxI* sandwich-like architecture, thus confirming the protein's ability to specifically adhere flat on the planar GO surface (Figure 4b). Besides these complexes, larger structures were found made by several overlapped GO-*SmPrxI* composites. Detailed imaging revealed multiple stacked GO layers coated by the *SmPrxI* rings, which were most likely acting as sticky moieties between the single layers, resulting in multi-layer architectures with variable heights rising up to several tens of nanometers (Figure 4c). Among the larger complexes, huge micrometric structures with amorphous architecture were observed. In this case, the multi-layer organization was very unclear, most likely because of the resolution limit of the scanning tip. For the same reason, both the single GO layers and the *SmPrxI* rings were not visible and the overall complexes appeared with an apparent multi-lobate organization showing height values up to hundreds of nanometers (Figure 4d).

In order to study the chemical interaction between the *SmPrxI* and the GO, X-ray photoelectron spectroscopy (XPS) was carried out on GO, *SmPrxI* and the GO-*SmPrxI* composite. In Figure 4e-f the C 1s core level spectra of GO before and after interaction with *SmPrxI*, and the S 2p core level spectra of the *SmPrxI* before and after interaction with GO are reported. The GO C 1s core level spectra were fitted by summing four components assigned respectively to aromatic sp² carbon (C-C), epoxy and hydroxyl groups (C-O), carbonyl groups (C=O) and carboxyl groups (C=O(OH)).³³ The evolution of the C 1s and S 2p core level spectra after the GO-*SmPrxI* mixing shows that the GO was reduced while the *SmPrxI* was oxidized. In particular, in the C 1s spectra (Figure 4e), the relative abundance of carbon atoms belonging to C-O groups (epoxy and hydroxyl) decreased by 35% in the GO-*SmPrxI* composite with respect to the pristine GO (the contribution of the C 1s core level signals of *SmPrxI* were subtracted to those of the GO-*SmPrxI* material, see for more details Supplementary Figure 2). The evolution of the S 2p core level spectra showed, on the other hand, an oxidation of the *SmPrxI*. The S 2p level spectrum of pristine *SmPrxI* (Figure 4f) was characterized

by two separated doublets at a binding energy of 164.3 eV and 168.6 eV ($2p_{3/2}$ position) with a relative abundance of 63% and 27% respectively. The lower binding energy doublet was assigned to S atoms belonging both to the thioether and sulfoxide of methionine and to the thiols of cysteine, in agreement with literature^{34,35}. The higher binding energy doublet is compatible with S atoms belonging to methionine sulfone and cysteine sulfonic acids^{36,37}, suggesting that pristine *SmPrxI* has been partially oxidized during protein storage³⁸. After the interaction with GO, the S 2p spectrum of *SmPrxI* (Figure 4f) showed only one doublet at a binding energy of 169.3 eV ($2p_{3/2}$ position). This peak was again assigned to sulfone and sulfonic acid and proved that the interaction with GO completely oxidized the sulfur atoms in *SmPrxI*. More details on the XPS analysis are reported in the supporting materials (Supporting Figure 2).

3.3 Microporous network of the rGO-*SmPrxI* composite. 3D morphological features of the rGO-*SmPrxI* composite were explored by low-voltage scanning electron microscopy (SEM) analysis (Figure 5). To do this, the colloidal matter was freeze-dried before deposition onto a SiO₂ wafer and observed while performing an EDS elemental microanalysis. A thin and fragile film was obtained after freeze-drying a control protein-free GO sample (Figure 5a). SEM imaging revealed an amorphous continuous material with thickness spanning several micrometers and a clear wrinkled surface most likely due to several GO molecules lying in a layer-by-layer arrangement. The related EDS spectrum clearly revealed the X-ray signal from carbon at ~ 0.28 keV, confirming the presence of GO. Further, besides carbon a strong silicon signal at ~ 1.74 keV was detected due to the underlying SiO₂ substrate. The oxygen at ~ 0.52 keV was likely to be shared between GO and the substrate. The presence of other elements, namely sodium, potassium and chloride at ~ 1.04 , 2.1 and 2.6 keV, respectively, was ascribed to the buffer components (Figure 5a). On the other hand, freeze-drying the rGO-*SmPrxI* colloid produced a compact, freestanding and low-weight 3D aerogel-like material with a quite spherical shape. The cross-sectioned material observed under SEM showed a quite uniform porous-like 3D internal morphology. This overall organization encompassed a dense network of micro-sized sheets clearly made by several stacked rGO layers forming the wall boundaries around the pores whose diameters were in the range of ~ 5 -10 μm . In agreement with the AFM images (see Figure 4c), such a hollow multi-layered framework suggested the presence of annealed sheets likely cross-linked to each other by the *SmPrxI* rings, the latter not visible by SEM due to the absence of staining and the resolution limit of the system. However, EDS microanalysis

showed an appreciable amount of sulfur at ~ 2.3 keV and nitrogen at ~ 0.39 keV, both undoubtedly ascribable to the protein's amino acid components (Figure 5b). Carbon density measurements revealed that the final dried rGO-*SmPrxI* weight was about 1.5 mg cm^{-3} , thus within the range of ultra-low GO networks ($0.2\text{-}4 \text{ mg cm}^{-3}$)³⁹. The 3D multi-layer architecture was found to be stable even after exposing the dried material to air for several weeks.

In view of the possible use of rGO-*SmPrxI* as a functionalized material doped with metal ions and with the goal to produce *in situ* assembled metal nanoparticles, we checked whether following chemical reduction treatment with NaBH_4 before freeze-drying, rGO-*SmPrxI* can maintain a 3D multi-layer architecture. We observed this architecture to be stable even under strong reducing conditions (Supporting Figure 3), even though this procedure caused partial breaking of the colloidal composite during incubation. On the contrary, the protein-free GO sample under strong reducing conditions, although forming a 3D structure, revealed a disordered microporous architecture by SEM analysis, with very rough stacking between layers (Supporting Figure 4).

3.4 Trapping AuNPs inside the rGO-*SmPrxI* composite. Given the ability of *SmPrxI* to induce gelation of GO (see Figure 4a) and create a 3D microporous composite (see Figure 5b), an additional step was performed in order to dope this material with presynthesized AuNPs. For this purpose, commercial 1.8 nm Ni^{2+} -functionalized AuNPs were conjugated to the histidine-fused *SmPrxI* rings (see Figure 1d) in presence of low concentrations of imidazole by exploiting the strong histidine- Ni^{2+} interaction, a strategy already proven to lead the AuNPs binding inside the *SmPrxI* lumen²⁶. AuNPs dissolved in aqueous buffer formed a brownish solution with a wide absorbance spectrum typical of gold nanoparticles (see Supporting Figure 5), as reported⁴⁰. After addition of *SmPrxI* (1AuNP per protein ring) the solution remained soluble without undergoing aggregation and showed a complex absorbance spectrum with the typical 280 and 230 nm protein signals. As for the rGO-*SmPrxI* sample (see Figure 4a), subsequent addition of GO to the *SmPrxI*-AuNPs mixture immediately triggered the formation of colloidal particles which underwent clumping to form a dark brown colloid aggregate, showing an internal microporous architecture after freeze-drying (Supporting Figure 6), thus achieving full phase separation and clarification of the supernatant. This led to almost zeroing of the final absorbance signal of all the components, namely AuNPs, *SmPrxI* and rGO, a clear indication of co-precipitation. Moreover, even after washing the pellet only a small absorbance was detected indicating that the AuNPs were stably trapped inside the rGO-*SmPrxI*

colloid (Supporting Figure 5a). To assess the role of *SmPrxI* acting as both AuNPs-specific bridges and sticky moieties, control mixing experiments were performed in the absence of protein. Under these conditions, no significant GO clumping, and thus no changes in the optical absorbance, was observed throughout incubation with AuNPs. Furthermore, even when GO was forcibly pulled down through ultracentrifugation and addition of NaCl the residual supernatant still exhibited almost full AuNPs absorbance signal, indicating that they were unable to directly adsorb on GO (Supporting Figure 5b).

High resolution TEM and STEM analysis were used to investigate the presence of AuNPs attached to the surface of the rGO-*SmPrxI* hybrid (Figure 6). In agreement with the spectroscopic analysis (see Supporting Figure 5), AuNPs did not bind to protein-free GO flakes deposited by drop casting onto holey carbon grid (Figure 6a) and chemical reduction led to a quite microporous though disordered architecture (data not shown). On the contrary the rGO-*SmPrxI*-AuNPs colloidal particles under low magnification STEM micrographs showed large GO complexes appearing as a network of stacked and cross-linked layers (Figure 6b), in agreement with the AFM images (see Figure 4b-d). High magnification TEM and STEM images clearly confirmed the decoration of the rGO flakes by heavier metal nanoparticles visible with darker and brighter contrast, respectively (Fig. 6b-d). By contrast, only a few were found attached to the underlying holey grid substrate where an individual GO flake over the amorphous carbon substrate of the grid was clearly selectively decorated by metal nanoparticles (Figure 6c). The corresponding EDS spectrum collected over the area revealed silicon and copper signals which originates from the materials composing the TEM grid, while the specific peaks from gold were visible, coming from the AuNPs on the flakes. The estimated density of AuNPs, measured by computer-aided approach, onto the *SmPrxI*-decorated rGO surface ($0.0023 \pm 0.0008 \text{ nm}^{-2}$) observed in the STEM/TEM micrographs was in good agreement with that of the *SmPrxI* rings bound onto the GO surface measured by AFM ($0.001 \pm 0.0003 \text{ nm}^{-2}$), considering that TEM, differently to AFM, do not discriminate between NPs bound above or below the single GO plane and thus the density resulting from TEM micrographs must be divided by two. The modality of AuNP binding to *SmPrxI* is shown in the TEM micrograph reported in Fig. 6d (lower panel). High-resolution TEM (HRTEM) images of the metal nanoparticles (Supporting Figure 7) clearly showed nanoparticle lattices fringes spaced by 0.235 nm, from gold (100) planes. Interestingly, the 3D microporous multi-layer architecture of the rGO-*SmPrxI*-AuNPs sample remained almost unchanged if treated by

freeze-drying, and the EDS spectrum at the SEM showed signals from gold at ~ 2.2 and 9.7 keV, as well as sulfur and nitrogen indicating the presence of both AuNPs and *SmPrxI* (see Supporting Figure 6). Furthermore, also the reduction with NaBH_4 did not alter significantly the 3D architecture of the rGO-*SmPrxI*-AuNPs material, indicating very a stable conformation (Supporting Figure 8).

3.5 *SmPrxI*-mediated synthesis of PdNPs into 3D rGO. The ability of the histidine-fused *SmPrxI* ring to bind Pd^{2+} ions was investigated through a TGA- Pd^{2+} spectroscopic assay (Supporting Figure 9). Upon mixing $(\text{NH}_4)_2\text{PdCl}_4$ with *SmPrxI* ($>1600\text{Pd}^{2+}$ per protein ring) the mixture instantly clumped, forming a pale yellow pellet which could be fractionated by ultra-centrifugation. The resulting supernatant used in the TGA assay showed an absorbance signal at 383 nm quenched to $\sim 60\%$ with respect to the protein-free $(\text{NH}_4)_2\text{PdCl}_4$ reference solution, meaning that a large amount of soluble Pd^{2+} ions, corresponding to $>900\text{Pd}^{2+}$ per protein ring, co-precipitated with *SmPrxI*. Very little absorbance was recorded when assessing the pellet after exhaustive washing, implying that the Pd^{2+} ions were not easily released likely because they were strongly attached to the protein forming the pellet (data not shown). A control assay was carried out on a protein-free GO- Pd^{2+} mixture. In this case, some clumping of GO clearly occurred upon mixing with $(\text{NH}_4)_2\text{PdCl}_4$ and the following ultra-centrifugation step led to a dark brown pellet. The TGA- Pd^{2+} spectroscopic assay performed on the supernatant revealed a $\sim 20\%$ absorbance quenching indicating that Pd^{2+} was partially adsorbed on GO. However, after washing the pellet and assessing the supernatant, a prominent absorbance signal was recovered suggesting that such a GO- Pd^{2+} interaction was not as strong as in the absence of protein (data not shown). To confirm this hypothesis, the assay was performed on an rGO-*SmPrxI*- Pd^{2+} mixture. In this case, before reacting with GO, the *SmPrxI*- Pd^{2+} complexes were required to be soluble. This condition was successfully achieved by adding imidazole to the reaction mix in order to modulate the binding between *SmPrxI* and the metal species avoiding their co-precipitation (see above), as previously described.²⁶ As for *SmPrxI* alone, the composite was able to stably bind Pd^{2+} with at least 800 Pd^{2+} ions per protein ring. Furthermore, extended incubation of GO within the *SmPrxI*- Pd^{2+} mixture caused the formation of an aggregate, meaning that *SmPrxI* retained its adhesive behavior for GO even when the metal was preloaded. After washing the so-formed composite, no significant release of the metal was observed (data not shown). Otherwise, only a weak adoption of Pd^{2+} was observed without protein (Supporting Figure 9).

After establishing the ability of *SmPrxI* to capture Pd^{2+} ions and bring them inside the rGO-based composite, a chemical reduction treatment was carried out with NaBH_4 in an attempt to grow PdNPs directly on the rGO support. During incubation with the reducing agent the color of the rGO-*SmPrxI*- Pd^{2+} composite quickly turned from brown to dark grey suggesting that further reduction of the protein-reduced rGO occurred. To prove that Pd^{2+} underwent reduction too, the material was crumbled by shaking prior to dropping onto a holey carbon grid and observing by TEM and high-resolution STEM (Figure 7). Lower resolution TEM micrographs clearly showed multi-layer rGO flakes bundles that clearly appeared during high magnification STEM images selectively decorated with mono-disperse metal nanoparticles (Figure 7a). The mean diameter of these NPs was obtained by statistical analysis based on more than 200 counts and determined to be 3.3 nm (sd= 2.0 nm). However, contrary to the rGO-*SmPrxI*-AuNPs composite, a high and heterogeneous density of PdNPs density was observed ($0.012 \pm 0.009 \text{ nm}^{-1}$). This result can be ascribed to the presence of discrete clusters of amino acidic residues onto the protein surface,²³ primarily glutamate, aspartate and histidine, known to be capable to start metal NP nucleation.^{41,42} Thus, it is likely that Pd^{2+} ions bind also to the *SmPrxI* ring surface, other than in its histidine-engineered cavity, providing additional nucleation sites for PdNPs growth; this increases the actual number of NPs onto the surface and demonstrates the pivotal template role of the protein. Unfortunately, all the attempts aimed at visualizing the *SmPrxI*-PdNPs bound failed likely due to the NaBH_4 treatment, which, upon NP formation, may interfere with protein stability⁴³. HRTEM imaging of the metal clusters revealed lattice fringes from (111) palladium crystal planes, spaced by 0.225 nm, as shown in the fast Fourier transform (FFT) in the inset figure. EDS analysis on the rGO-NPs composites further confirmed that the nanoparticles were made of palladium (Figure 7b).

Additional TEM images collected at lower voltage confirmed the very homogeneous arrangement of the PdNPs covering almost the entire rGO layers (Figure 8a). Interestingly, incubation of Pd^{2+} with a preformed rGO-*SmPrxI* colloid followed by chemical reduction led to comparable results, indicating that even when encapsulated within the 3D rGO composite, the protein rings held their adsorption activity toward metal ions, as proven by TEM (Supporting Figure 10). As a control, the protein-free GO was analyzed after being incubated with Pd^{2+} , washed and reduced. Again, exposure to NaBH_4 clearly produced rGO as noticed by the color change, but no discrete PdNPs were found by TEM (Figure 8b) in agreement with the weak adsorption of Pd^{2+} on GO observed by spectroscopic assay (see Supporting Figure 9).

3.6 Discussion

Self-assembly of 3D graphene-based materials is inspiring an expanding volume of work, mostly because their synthesis represents an easy route to tailor and enhance the properties of 2D graphene to create more manageable structures suitable for practical applications. In this work, 3D rGO-based composites have been assembled and functionalized with metal NPs, by adsorbing a protein, *i.e.* *SmPrxI*, on single 2D GO layers. To the best of our knowledge this represents a unique “green” synthetic route to achieve assembly, chemical reduction and functionalization with metal NPs of graphene composites simply by using a single “multitasking” protein reagent.

The *SmPrxI* protein exists as a ring-like structure with a cysteine-dependent redox activity involved in intracellular reduction of peroxides.²³ Upon conformational change, the ring may also expose sticky hydrophobic surfaces at the rim of the cavity acquiring molecular chaperone activity (Figure 1c).^{24,25} Our data indicate that clumping of GO into aggregates can be readily triggered by *SmPrxI* (Figure 2 and 4a) both due to its identical and sticky surfaces (Figure 1b and 1c), a consequence of the *SmPrxI*'s “double-faced” structure and its molecular chaperone activity, as well as its reducing properties related to the sulfur-containing residues, *i.e.* cysteine and methionine (Figure 1c). These features operate synergistically to drive the stacking of the single GO layers into 3D composites. The 3D architecture of the so-formed composite clearly shows a microporous network of interconnected multi-layer GO sheets in which the *SmPrxI* rings are likely to occupy the interlayer space acting as both adhesive and spacer moieties (Figure 4b-d and 5b).

As shown by AFM (Figure 3), the *SmPrxI* rings stably adhere onto GO layers through a “face-on” mode of interaction (Figure 2); this is likely due to the larger contact surface involved with respect to an “edge-on” interaction, and by the sticky patches surrounding the *SmPrxI*'s lumen. As a direct consequence of their “double-faced” feature, the GO-bound rings can further interact with other GO molecules using the solvent-exposed surface; this occurs in solution resulting in GO layer stacking and aggregation (Figure 4a-d).

Concurrently, *SmPrxI* is capable to reduce GO, strengthening the 3D architecture by enhancing the hydrophobic π - π interactions between layers^{12,14,44}. A visual inspection of the *SmPrxI* crystallographic structure reveals that 50 cysteines and 60 methionines, these latter mostly present at the N-terminal tags of each decamer (Figure 1 and Supporting Figure 1), are exposed to the GO-*SmPrxI* interfaces and thus potentially capable to participate in the redox reaction between the

reactants. In fact, XPS spectra show striking formation of new C–C bonds in the GO to the detriment of its C–O bonds (Figure 4e) with concomitant oxidation of the protein's cysteine thiols and methionine thioethers to sulfonates and sulfones, respectively (Figure 4f). These results are in agreement with the known ability of some sulfur-containing compounds to effectively reduce GO by reducing its epoxide content.^{45,46,47} Given that the majority of proteins are characterized by sulfur-containing amino acids, the redox reaction hereby described for the first time, is likely to occur in any interface where proteins/enzymes and GO come in touch. As a matter of fact, Liu *et al.*²⁰ reported the possibility to adsorb different preformed metal NPs onto the GO by means of bovine serum albumin; they found that GO, upon albumin interaction, is reduced hypothesizing that the reaction is at the expense of the 20 tyrosines present in each monomer which oxidize to the quinone forms. However, analysing the sequence of bovine serum albumin (accession code: CAA76847), also 35 cysteines and 5 methionines are present per monomer; thus we can hypothesize that also in this case the reduction of GO is at least in part ascribable to the redox-active sulphur-containing amino acids of the protein similarly to what we found for the *SmPrxI*-GO interaction.

Overall, the assembly process is quickly accomplished under mild conditions, that is in aqueous solution, slightly basic pH (7.5) and room temperature, yet it requires very small amounts of both protein and GO, the latter well below the known critical concentrations for self-gelation, *i.e.* $\geq 3 \text{ mg ml}^{-1}$, as reported⁴⁴. To the best of our knowledge, there is no example of protein-induced self-assembly of GO at this very low concentration.

The solvent-accessible inner surface of the *SmPrxI* ring has been equipped, by modifying its N-termini, with 60 additional His and 40 Asp residues, creating a wide region of about 140 nm^3 spatially constrained inside the protein scaffold suitable for binding metal ions with high affinity (Figure 1d).²⁶ This region has been successfully exploited to dope the 3D rGO composite with metal NPs. To validate the proposed synthesis method and demonstrate its flexibility, either preformed Au or *in-situ* generated PdNPs were encapsulated within rGO (Figure 2). The procedures can be summarized as follows: (1) *SmPrxI* is incubated with Ni^{2+} -functionalized AuNPs or Pd^{2+} ions, (2) GO is then added to the protein-metal mixture, and (3) NaBH_4 is used to reduce Pd^{2+} to Pd^0 . Regardless of either AuNPs or $\text{Pd}^{2+}/\text{Pd}^0$, the protein retains the sticky behavior towards GO thus allowing a 3D material to be achieved. The ability of such polyHis-*SmPrxI* recombinant rings to capture and tether colloidal 1.8 nm Ni^{2+} -functionalized AuNPs has been previously demonstrated. The binding is ruled by the Ni^{2+} -His coordination bond and effectively brings the AuNPs into the ring center (Figure 6d).²⁶

This interaction leads the rGO composites to be doped with AuNPs (Figure 6b and 6c) as the latter are poorly adsorbed without the protein bridge (Figure 6a and Supporting Figure 5). The observed binding selectivity for the inner ring space shown by AuNPs is likely due to the presence of the 10 His-tags, clustered in the protein lumen, which have been specifically designed to bind nickel with nanomolar affinity⁴⁸. Moreover, the *SmPrxI* ring can also be exploited as a suitable scaffold for growth of PdNPs. By UV-Vis spectroscopy it is estimated that $\sim 800\text{Pd}^{2+}$ ions bind to the protein, likely both to its engineered N-terminal polyHis sequences at the inner surface, as also reported for similar proteins,^{49,50} and to the metal-binding amino acids natively present on the ring surface (see Figure 1d and Results). Contrary to what seen in the case of AuNPs that are specifically found inside the ring of *SmPrxI*, PdNPs are presumably located also on the protein surface, as demonstrated by the higher density of the latter measured by STEM/TEM techniques. The reduced specificity of the Pd^{2+} towards the *SmPrxI* inner cavity with respect to the AuNP can be ascribed to the higher concentrations of the former metal ions used to assemble the relative GO composite; indeed, in the preparation of rGO-*SmPrxI*-PdNPs, the protein is incubated with 1-2 mM of Pd^{2+} while in the case of rGO-*SmPrxI*-AuNPs the concentration of the preformed NPs is lower than 3 orders of magnitude. Accordingly, it is known that palladium ions are easily adsorbed onto protein surfaces even at lower concentration.⁵¹ Before the Pd^{2+} ions induce protein to aggregate,²⁶ the addition of GO to the mix yields a 3D rGO with Pd^{2+} ions trapped inside. Interestingly, the process of ion adsorption onto rGO through the protein moiety is very fast, requiring only a few minutes. This strongly confers to *SmPrxI* a pivotal role as metal bridge since GO itself seems to require long-term contact times, higher temperatures and higher Pd^{2+} concentrations to achieve similar results even after being modified with metal-binding functionalities.^{52,53} The following reduction step is necessary to form PdNPs with roundish shape and dimensions of about 3.3 nm (Figure 7 and 8a). This result could stand alone as a solution to avoid PdNPs-related difficulties such as aggregation, reduced activity, inferior selectivity, metal leaching and high preparation complexity.⁵³ Interestingly, it was also possible to use the preformed rGO-*SmPrxI* colloid as a metal-trapping material. In this case the metal has been added after formation of the 3D composite. The bound Pd^{2+} ions in the 3D GO array cannot be removed by extensive washing unlike those bound to GO alone which are easily removed by buffer exchanging. In this case, after reduction with NaBH_4 TEM analysis reveals that PdNPs can grow inside a preformed rGO-*SmPrxI* complex (Supporting Figure 10), suggesting the suitability of

its use as a working metal-trap. In fact, the use of 3D GO-related materials as metal sorbents for environmental protection is spreading worldwide.⁵⁴

4 Conclusions

By a single proteinaceous reactant, *i.e.* *SmPrxI*, it is possible to: (i) assemble 3D GO; (ii) reduce its surface; (iii) encapsulate preformed metal nanoparticle and (iv) allow the *in situ* growth of PdNPs; all these operations are carried out at ambient temperature, in water at pH 7.5 and using very small amounts of GO. The reduction capability of a protein towards GO was demonstrated to be dependent on its sulfur-containing amino acids. Considering that the majority of proteins contain several cysteines and/or methionines, each time a protein or an enzyme is adsorbed onto the GO, *e.g.* to approach biosensors, the redox reaction hereby described must be taken into account. Moreover, the metal-binding peptides fused within the *SmPrxI* cavity are known to tether several other metal ions such as cobalt, zinc, iron, and copper with nM affinity⁵⁰, further highlighting the outstanding potential of the rGO-*SmPrxI* material both as a platform to assemble GO/rGO-NPs composites and as a metal-scavenging material. In conclusion, we believe that our bio-composite rGO-*SmPrxI* may represent an innovative "green" system to obtain a flexible, scalable and selective material with diverse applications in the fields of chemical catalysis, opto-electronics, environmental recovery and possibly bio-scaffold generation.

Acknowledgments

This work was partially supported by the University of L'Aquila (R.I.A. ex 60% to F.A. and R.I.). We acknowledge Dr. Lorenzo Arrizza and Dr. Maria Giammatteo of the Microscopy Centre of the University of L'Aquila for technical assistance.

Author contributions

M. Ardini made biochemical experiments and sample preparations for all microscopic analysis and made part of the AFM and TEM measurements and analyses. G. Golia, P. Passaretti, L. Di Leandro, F. Giansanti, G. Pitari and A. Cimini gave contributions to the preparation of proteins and the characterization of metal binding. L. Ottaviano. S. Santucci and F. Perrozzi realized XPS, SEM and

AFM measurements. V. Morandi, L. Ortolani and M. Christian made STEM, TEM and EDS analysis. V. Palermo and E. Treossi prepared the GO. M. Ardini, F. Angelucci and R. Ippoliti decided experiments and wrote the paper with input from all the authors. F. Angelucci and R. Ippoliti conceived and supervised the research.

Competing financial interests

The authors declare no competing financial interests.

Footnotes.

Electronic supporting information is available:

Supp. Fig. 1: SmPrxI amino acid sequence engineered with the N-terminal metal-binding sequence

Supp. Fig. 2: XPS C 1s and S 2p core level spectra of GO, Prx and GO+Prx

Supp. Fig. 3: SEM images of chemically reduced rGO-SmPrxI

Supp. Fig. 4: SEM images of chemically reduced GO

Supp. Fig. 5: UV-Vis spectra SmPrxI-mediated adsorption of AuNPs on rGO

Supp. Fig. 6: SEM images and EDS analysis of rGO-SmPrxI-AuNPs

Supp. Fig. 7: HRTEM micrographs of commercial Ni²⁺-functionalized AuNPs

Supp. Fig. 8: SEM images of chemically reduced rGO-SmPrxI-AuNPs

Supp. Fig. 9: UV-Vis spectra of Pd²⁺ adsorption by rGO-SmPrxI

Supp. Fig. 10: TEM micrographs of chemically reduced rGO-SmPrxI after interaction with Pd²⁺

References

1. K.S. Novoselov, A.K. Geim, S.V. Morozov, D. Jiang, Y. Zhang, S.V. Dubonos, I.V. Grigorieva and A.A. Firsov, *Science*, 2004, **306**, 666.
2. X. Xiao, T.E. Beechem, M.T. Brumbach, T.N. Lambert, D.J. Davis, J.R. Michael, C.M. Washburn, J. Wang, S.M. Brozik, D.R. Wheeler, D.B. Burckel and R. Polsky, *ACS Nano*, 2012, **6**, 3573.
3. C. Lee, X. Wei, J.W. Kysar and J. Hone, *Science*, 2008, **321**, 385-388.
4. K.I. Bolotin, K.J. Sikes, Z. Jiang, M. Klima, G. Fudenberg, J. Hone, P. Kim and H.L. Stormer, *Solid State Commun.*, 2008, **146**, 351.
5. A.A. Balandin, S. Ghosh, W. Bao, I. Calizo, D. Teweldebrhan, F. Miao and C.N. Lau, *Nano Lett.*, 2008, **8**, 902.
6. X. Huang, Z. Yin, S. Wu, X. Qi, Q. He, Q. Zhang, Q. Yan, F. Boey and H. Zhang, *Small*, 2011, **7**, 1876.
7. F. Perrozzi, S. Prezioso and L. Ottaviano, *J. Phys. Cond. Matter*, 2015, **27**, 013002.
8. S. Prezioso, F. Perrozzi, L. Giancaterini, C. Cantalini, E. Treossi, V. Palermo, M. Nardone, S. Santucci and L. Ottaviano, *J. Phys. Chem. C*, 2013, **117**, 10683.
9. Y. Zhu, S. Murali, W. Cai, X. Li, J.W. Suk, J.R. Potts and R.S. Ruoff, *Adv Mater.*, 2010, **22**, 3906.
10. A. Bianco, *Angew. Chem., Int. Ed.*, 2013, **52**, 4986.
11. S. Pei and H. Cheng, *Carbon*, 2012, **50**, 3210.
12. R.L.D. Whitby, *ACS Nano*, 2014, **8**, 9733.
13. M. Zeng, W. Wang and X. Bai, *Chin. Phys. B*, 2013, **22**, 098105.
14. Y. Xu, Q. Wu, Y. Sun, H. Bai and G. Shi, *ACS Nano*, 2010, **4**, 7358.
15. Y. Xu, Z. Lin, X. Huang, Y. Wang, Y. Huang and X. Duan, *Adv. Mater.*, 2013, **25**, 5779.
16. S. Ahadian, M. Estili, V.J. Surya, J. Ramón-Azcón, X. Liang, H. Shiku, M. Ramalingam, T. Matsue, Y. Sakka, H. Bae, K. Nakajima, Y. Kawazoe and A. Khademhosseini, *Nanoscale*. 2015 **7**, 6436.
17. Z. Xia, D. Wei, E. Anitowska, V. Bellani, L. Ortolani, V. Morandi, M. Gazzano, A. Zanelli, S. Borini and V. Palermo, *Carbon*, 2015, **84**, 254.
18. J.J. Shao, W. Lv and Q.H. Yang, *Adv. Mater.*, 2014, **26**, 5586.

19. Z. Wang, X. Lv, Y. Chen, D. Liu, X. Xu, G.T. Palmore and R.H. Hurt, *Nanoscale*, 2015, **7**, 10267.
20. J. Liu, S. Fu, B. Yuan, Y. Li and Z. Deng, *J. Am. Chem. Soc.*, 2010, **132**, 7279.
21. J. Lin, T. Mei, M. Lv, C. Zhang, Z. Zhao and X. Wang, *RSC Adv.*, 2014, **4**, 29563.
22. Y. Zhang, C. Wu, S. Guo and J. Zhang, *Nanotechnol. Rev.*, 2013, **2**, 27.
23. F. Saccoccia, P. Di Micco, G. Boumis, M. Brunori, I. Koutris, A.E. Miele, V. Morea, P. Sriratana, D.L. Williams, A. Bellelli and F. Angelucci, *Structure*, 2012, **20**, 429.
24. F. Angelucci, F. Saccoccia, M. Ardini, G. Boumis, M. Brunori, L. Di Leandro, R. Ippoliti, A.E. Miele, G. Natoli, S. Scotti and A. Bellelli, *J. Mol. Biol.*, 2013, **425**, 4556.
25. F. Angelucci, A. Bellelli, M. Ardini, R. Ippoliti, F. Saccoccia and V. Morea, *Febs J.*, 2015, **282**, 2827.
26. M. Ardini, F. Giansanti, L. Di Leandro, G. Pitari, A. Cimini, L. Ottaviano, M. Donarelli, S. Santucci, F. Angelucci and R. Ippoliti, *Nanoscale*, 2014, **6**, 8052.
27. E. Treossi, M. Melucci, A. Liscio, M. Gazzano, P. Samorile and V. Palermo, *J. Am. Chem. Soc.*, 2009, **131**, 15576.
28. B. Mathew and D. Innocent, *Asian J. Chem.*, 2010, **22**, 7551.
29. L. Liu, C. Li, C. Bao, Q. Jia, P. Xiao, X. Liu and Q. Zhang, *Talanta*, 2012, **93**, 350.
30. D. Pandey, R. Reifengerger and R. Piner, *Surf. Sci.*, 2008, **602**, 1607.
31. D. Ricci and P.C. Braga, *Atomic Force Microscopy: Biomedical Methods and Applications*, Humana Press, Totowa, New Jersey, USA, 2004.
32. A. Engel, B. Baumeister and W.O. Saxton, *Proc. Natl. Acad. Sci.*, 1982, **79**, 4050.
33. F. Perrozzi, S. Prezioso, M. Donarelli, F. Bisti, P. De Marco, S. Santucci, M. Nardone, E. Treossi, V. Palermo and L. Ottaviano, *J. Phys. Chem. C*, 2013, **117**, 620.
34. S.R. Kelemen, G.N. George and M.L. Gorbaty, *Fuel*, 1990, **69**, 939.
35. X.R. Yu, F. Liu, Z.Y. Wang and Y. Chen, *J. Electron Spectrosc. Relat. Phenom.*, 1990, **50**, 159.
36. B.J. Lindberg, K. Hamrin, G. Johansson, U. Gelius, A. Fahlman, C. Nordling and K. Siegbahn, *Phys. Scripta*, 1970, **1**, 286.
37. X.L. Wei, M. Fahlman and A.J. Epstein, *Macromolecules*, 1999, **32**, 3114.
38. E.R. Stadtman, *Annu. Rev. Biochem.*, 1993, **62**, 797.

39. V. Chabot, D. Higgins, A. Yu, X. Xiao, Z. Chen and J. Zhang, *Energy Environ. Sci.*, 2014, **7**, 1564.
40. J.F. Hainfeld and F.R. Furuya, *J. Histochem. Cytochem.*, 1992, **40**, 177.
41. J. Bhattacharya, S. Jasrapuria, T. Sarkar, R. GhoshMoulick and A.K. Dasgupta, *Nanomedicine* 2007, **3**, 14.
42. H. Wei, Z. Wang, J. Zhang, S. House, Y.G. Gao, L. Yang, H. Robinson, L.H. Tan, H. Xing, C. Hou, I.M. Robertson, J.M. Zuo and Y. Lu, *Nat. Nanotechnol.*, 2011, **6**, 93.
43. M.A. Paz, E. Henson, R. Rombauer, L. Abrash, O.O. Blumenfeld and P.M. Gallop, *Biochemistry*, 1970, **9**, 2123.
44. H. Bai, C. Li, X. Wang and G. Shi, *J. Phys. Chem.*, 2011, **115**, 5545.
45. D.R. Dreyer, H. Jia, A.D. Todd, J. Geng and C.W. Bielawski, *Org. Biomol. Chem.*, 2011, **9**, 7292.
46. W. Chen, Y. Yan and P.R. Bangal, *J. Phys. Chem. C*, 2010, **114**, 19885.
47. D. Chen, L. Li and L. Guo, *Nanotechnology*, 2011, **22**, 325601.
48. S. Knecht, D. Ricklin, A.N. Eberle and B. Ernst, *J. Mol. Recognit.*, 2009, **22**, 270.
49. R.A. McMillan, J. Howard, N.J. Zaluzec, H.K. Kagawa, R. Mogul, Y.F. Li, C.D. Paavola and J.D. Trent, *J. Am. Chem. Soc.*, 2005, **127**, 2800.
50. S. Behrens, A. Heyman, R. Maul, S. Essig, S. Steigerwald, A. Quintilla, W. Wenzel, J. Bürck, O. Dgany and O. Shoseyov, *Adv. Mater.*, 2009, **21**, 3515.
51. S. Abe, T. Hikage, Y. Watanabe, S. Kitagawa and T. Ueno, *Inorg. Chem.*, 2010, **49**, 6967.
52. L. Liu, S. Liu, Q. Zhang, C. Li, C. Bao, X. Liu and P. Xiao, *J. Chem. Eng. Data*, 2013, **58**, 209.
53. C. Bai, Q. Zhao, L. Yang, G. Zhang, F. Zhang and X. Fan, *Catal. Lett.*, 2014, **144**, 1617.
54. M. Lü, J. Li, X.Y. Yang, C.A. Zhang, J. Yang, H. Hu and X.B. Wang, *Chin. Sci. Bull.*, 2013, **58**, 2698.

Figure Legends

Figure 1. Main properties of *SmPrxI*. **a)** The ring-like *SmPrxI* complex is made by 5 homodimers with their 180° axis perpendicular to the ring 5-fold rotational axis. **b)** The complex has a thickness, internal and external diameter of ~5, 6 and 13 nm, respectively. This assembly confers a “double-faced” appearance, as the exposed surfaces at the top and bottom of the ring plane are equivalent. **c)** These surfaces are endowed with sulfur-containing amino acids, namely cysteines and methionines (in yellow) and hydrophobic patches (in grey). **d)** The putative metal binding sites of *SmPrxI* are highlighted in red. *SmPrxI* is engineered to contain an additional histidine-rich sequence at the N-terminus of each subunit lying at the ring’s cavity (see Supporting Figure 1). These sequences do not alter the ring's quaternary structure while exhibiting high affinity for divalent metal cations. These metal binding sites are additional to those natively present on the ring surface constituted by amino acids such as glutamic/aspartic acids and histidines shown in red sticks.

Figure 2. Scheme of the proposed method. **a)** The *SmPrxI* rings adhere flat over the smooth planar surface of single GO layers and partially reduce them to induce self-assembly of a 3D multi-layer rGO-*SmPrxI* hybrid composite. **b)** The same approach is exploited to obtain an rGO-*SmPrxI*-AuNPs composite. In this case, the protein is pre-conjugated with Ni²⁺-functionalized AuNPs through the interaction between the N-terminal histidine-rich binding sites and the Ni²⁺ ions. **c)** Likewise, the same interaction, together with the capability of protein surfaces to capture metal ions, is exploited to stably trap Pd²⁺ ions onto the ring template prior to chemical reduction towards an rGO-*SmPrxI*-PdNPs material.

Figure 3. GO-*SmPrxI* complexes assembled on substrate. **a)** AFM images of spin-coated GO show single or partially overlapped layers. Zoom details reveal their typical smooth planar surface with height profile (estimated along the white line) of ~0.9-1 nm. **b)** After dropping *SmPrxI*, the layered structure of GO is not altered, but its surface becomes highly pitted due to the presence of many protein particles with ~5.1 height and ~20 nm width, according to the dimensions of the *SmPrxI* ring-like structure (see Figure 1b; PDB code: 3ZTL). Given the protein coating the height profile of the resulting GO-*SmPrxI* complexes increases to ~6 nm on average (scale bars= 500 nm). **c)** STEM images of individual *SmPrxI* rings over GO (scale bars= 40 nm).

Figure 4. Stacking and reduction of GO by *SmPrxI*. **a)** GO remains soluble in aqueous buffer at pH 7.5. Upon mixing with *SmPrxI*, it quickly clumps forming visible colloidal particles. Such particles self-assemble within 60 min leading to a freestanding hydrogel-like colloid which is easily broken by shaking though retaining its self-assembly ability to form the aggregate again. The broad optical absorbance of GO is scattered upon mixing with *SmPrxI* due to the particle formation and progressively decreases as the clumps sink to the bottom of the cuvette forming the colloid. At the end of the process neither GO nor *SmPrxI* absorbance are significant suggesting they are co-precipitated. The insert illustrates the kinetic trend of the GO absorbance at 400 nm. **b)** AFM analysis on the clumped particles shows a heterogeneous population of GO-*SmPrxI* hybrid composites. The smallest are single or partially overlapped GO layers. Details reveal the presence of a *SmPrxI* coat making the layer surface highly rough with height ~ 10 nm pointing to a *SmPrxI*-GO-*SmPrxI* sandwich-like architecture (scale bar= 300 nm). **c)** Larger composites are found made by stacked multi-layer GO-*SmPrxI* hybrids where each layer appears covered by several protein rings. Such organization increases the height value to several tens of nanometers (scale bar= 1 μm). **d)** Very large complexes with amorphous lobate-like architecture are also observed. Due to their dimensions, both the GO layers and the *SmPrxI* rings as well as the multi-layer organization are not distinguishable probably because of the low resolution of the scanning tip. These structures show height values of several hundreds of nanometers (scale bar= 1 μm). **e)** XPS C 1s core level spectra of GO (upper spectrum) and XPS C 1s core level spectra of reduced GO calculated from the C 1s spectra acquired on the GO+*SmPrxI* sample (lower spectrum); the contribution of the C 1s core level signals of *SmPrxI* were subtracted from both spectra (See Supplementary Figure 2 for more details). **f)** XPS S 2p core level spectra of *SmPrxI* (upper spectrum) and XPS S 2p core level spectra of GO+*SmPrxI* (lower spectrum).

Figure 5. 3D morphological features of the rGO-*SmPrxI* composite. **a)** Freeze-dried GO is imaged as a thin amorphous film under SEM. Zoom details show wrinkles randomly arranged on the carbon surface indicating several overlapped GO layers. The X-ray spectrum from EDS microanalysis proves the carbon and oxygen content in the dried matter at ~ 0.28 and ~ 0.52 keV, respectively, besides the substrate and buffer components. **b)** The freeze-dried rGO-*SmPrxI* composite is a soft, compact, freestanding material capable of being manipulated by tweezers. It has an internal

microporous architecture with $\sim 5\text{-}10\ \mu\text{m}$ cavities whose boundaries are made by multi-layer rGO sheets of several stacked layers. The presence of *SmPrxI* (not visible without staining) inside the porous network is confirmed by the EDS signals from nitrogen and sulfur at ~ 0.39 and ~ 2.3 keV, respectively, which unambiguously belong to the protein (scale bars= $10\ \mu\text{m}$).

Figure 6. STEM and HRTEM analysis of *SmPrxI*-mediated functionalization of rGO with AuNPs.

a) STEM images of the AuNPs deposited on rGO layers (scale bars= 100 and $20\ \text{nm}$).

Nanoparticles are visible as single shiny spots with $2\ \text{nm}$ diameter evenly and randomly distributed.

b) STEM micrograph showing the rGO-*SmPrxI* complexes forming multi-layers complexes over the holey carbon film of the TEM grid. Higher magnification images shows the nanoparticle decoration of the rGO flakes (scale bars= $2\ \mu\text{m}$ and $50\ \text{nm}$).

c) STEM image of an individual rGO flake over the amorphous carbon film of the grid, showing selective decoration with AuNPs (scale bar= $50\ \text{nm}$).

The presence of gold is proven by EDS analysis performed over the area. **d)** HRTEM image of the AuNPs onto the rGO surface in presence of *SmPrxI* without protein staining (upper panel, scale bar= $4\ \text{nm}$). The AuNP within the *SmPrxI* ring after protein staining with uranyl acetate is shown (lower panel, scale bar= $20\ \text{nm}$).

Figure 7. STEM analysis of *SmPrxI*-mediated PdNPs on the rGO support.

a) TEM image of the GO-*SmPrxI*-Pd composites over a holey carbon grid (left panel, scale bar= $1\ \mu\text{m}$). Selective metal nanocluster decoration is evident by STEM at high magnification (right panel, scale bar= $50\ \text{nm}$).

b) HRTEM image of several nanoclusters, showing Pd lattice fringes (scale bar= $5\ \text{nm}$). (inset) FFT of the image, with Pd (111) reflections, corresponding to $0.225\ \text{nm}$, are highlighted and the (200) ring at $0.194\ \text{nm}$ is clearly visible. EDS confirms the chemical nature of such found NPs revealing the presence of a remarkable palladium amount at $\sim 2.84\ \text{keV}$ besides the protein's typical components such as sulfur and nitrogen.

Figure 8. TEM analysis of *SmPrxI*-mediated PdNPs on the rGO support.

a) The PdNPs grow on *SmPrxI* such that the final composite material shows a very homogeneous arrangement of mono-disperse NPs spreading on the rGO flakes and forming only very few amorphous aggregates (left panel scale bar= $1\ \mu\text{m}$; right panel scale bar= $100\ \text{nm}$).

b) TEM micrographs of chemically reduced GO after interaction with Pd^{2+} without *SmPrxI*. PdNPs are not visible in the 3D GO, demonstrating

that the GO alone is not able to effectively retain Pd²⁺ (left panel scale bar= 1 μm; right panel scale bar= 100 nm). The images were collected with CM-100 electron microscope (Philips) equipped with a tungsten filament operating at 80 kV.